Mathematical Biosciences and Engineering

http://www.aimspress.com/journal/mbe

MBE, 20(3): 4643–4672.
DOI: 10.3934/mbe.2023215
Received: 01 November 2022
Revised: 15 December 2022
Accepted: 17 December 2022
Published: 28 December 2022

Research article

A numerical study of COVID-19 epidemic model with vaccination and diffusion

Ahmed Alshehri[1] **and Saif Ullah**[2,*]

[1] Department of Mathematics, Faculty of Sciences, King Abdulaziz University, Jeddah 21589, Saudi Arabia

[2] Department of Mathematics, University of Peshawar, Khyber Pakhtunkhwa, Pakistan

* **Correspondence:** Email: saifullah.maths@uop.edu.pk.

Abstract: The coronavirus infectious disease (or COVID-19) is a severe respiratory illness. Although the infection incidence decreased significantly, still it remains a major panic for human health and the global economy. The spatial movement of the population from one region to another remains one of the major causes of the spread of the infection. In the literature, most of the COVID-19 models have been constructed with only temporal effects. In this paper, a vaccinated spatio-temporal COVID-19 mathematical model is developed to study the impact of vaccines and other interventions on the disease dynamics in a spatially heterogeneous environment. Initially, some of the basic mathematical properties including existence, uniqueness, positivity, and boundedness of the diffusive vaccinated models are analyzed. The model equilibria and the basic reproductive number are presented. Further, based upon the uniform and non-uniform initial conditions, the spatio-temporal COVID-19 mathematical model is solved numerically using finite difference operator-splitting scheme. Furthermore, detailed simulation results are presented in order to visualize the impact of vaccination and other model key parameters with and without diffusion on the pandemic incidence. The obtained results reveal that the suggested intervention with diffusion has a significant impact on the disease dynamics and its control.

Keywords: space-time COVID-19 transmission model; finite difference operator-splitting scheme; existence and uniqueness; numerical simulation

1. Introduction

The COVID-19 pandemic is a global outbreak, caused by the severe acute respiratory syndrome coronavirus 2 (SARS-CoV-2) [1]. This infection is highly contagious and is transmittable from person to person via respiratory droplets, produce as a consequence of coughing and sneezing of an infectious person. Although the severity and mortality rate of this novel infection is notably reduced, still it is

a huge panic for human health as well as economy around the globe. This infection is still the main cause of restricting lives of humans in many regions. Despite huge research on this novel disease, scientists are focusing to explore its different aspects. According to recent statistics, more than 621.8 million infected cases are reported globally. Out of the total reported infected cases about 6.5 million death cases and about 601.9 million recovered cases are recorded [1]. Many pharmaceutical and non-pharmaceutical preventing strategies were suggested and implemented to overcome the infection. For instance, taking vaccines, staying at home, usage of facemasks specifically in public areas, avoiding crowded places, etc [1, 2].

One of the main causes of the infection spread is the spatial movement of population from one region to another. The assessment of geographical spreading patterns as well as the impact of those factors causing the transmission and eradication of infection can be carried out using mathematical models [3–7]. In existing literature, most of COVID-19 epidemic models have been constructed via ordinary differential equations (ODEs). In contrast to ODEs models, the mathematical models based on PDEs, particularly the reaction-diffusion is more appropriate and have promising results describing the dynamics of an infectious disease. Numerous mathematical spatio-temporal epidemic models have been developed to explore the transmission patrons of various infectious diseases including COVID-19. These problems were solved numerically using different numerical techniques to analyze the dynamics of different infectious and viral diseases. Such as, in [8] the authors formulated a reaction-diffusion deterministic model to analyze the spatio-temporal dynamics of influenza. They further utilized the finite-difference scheme in order to visualize the disease dynamics. In [9], the authors developed a diffusive vaccine epidemic model with variable transmission coefficient addressing the spatio-temporal dynamical aspects of influenza disease. Moreover, in [9] the authors presented a detailed analysis of the model. A compartmental spatio-temporal epidemic model is considered by Jawaz et al. [10], for investigating the complex dynamics of HIV/AIDS and proposed the non-standard finite difference numerical technique for the solution due to its positivity preserving property. Ahmed et al. [11], discussed the numerical solution of the whooping cough epidemic model by using an operator-splitting finite difference scheme. The numerical techniques, operator-splitting based finite difference and meshless prodedures have been used for solving the spatio-temporal epidemic models in Refs. [12, 13]. Asif et al. [14] discussed the approximate solution of two spatio-temporal biological models by using meshless and finite difference procedures based on operator splitting techniques. A structure-preserving non-standard finite difference operator-splitting procedure has been implemented by Ahmed et al. [15], to obtain the numerical solution of the reaction-diffusion epidemic model. Sokolovsky et al. [16] examined analytic and numerical solution of spatio-temporal epidemiological models and analyze different stages of the epidemic. A novel reaction-diffusion model describing the dynamics of COVID-19 is developed in [17]. A reaction-diffusive spatial model addressing the dynamics of pandemic in Greece and Andalusia as a case study is presented in [18].

In this paper, we present a spatio-temporal vaccine mathematical model to address the dynamics of COVID-19 in a spatially heterogeneous environment. The model is actually the spatial extension of [19]. Initially, we present some basic and necessary mathematical properties of the proposed spatio-temporal model. The model is then solved numerically using an efficient numerical scheme to present the simulation results. The paper outlines are categorized as: Section 2 describes the formulation of spatio-temporal model. A basic mathematical analysis of the problem is presented in Section 3. Numerical solution of the model and detailed simulation with and with diffusion is investigated in

Section 4. Finally, the concluding remarks are summarized in Section 5.

2. Spatio-temporal COVID-19 model description

In this section, a compartmental epidemic reaction-diffusion model is formulated in order to analyze temporal and spatial dynamics of COVID-19 outbreak. The total population at time $t \geq 0$ and spatial point $x \in [-2, 2]$ is denoted by $\mathcal{N}(x,t)$ and assumed to be constant i.e., in the population birth and deaths rates are equal. The population $N(x,t)$ is further categorized into sub-classes denoted by $S(x,t), E(x,t), I_S(x,t), I_A(x,t), V(x,t)$ and $R(x,t)$ describing the susceptible, latent, symptomatically, asymptomatically, vaccinated and recovered population groups respectively. The spatial distribution of total available population at time $t \geq 0$ and $x \in \Xi = [-2, 2]$ is

$$\mathcal{N}(t) = \int_{\Xi} \Big\{ S(x,t) + E(x,t) + I_S(x,t) + I_A(x,t) + V(x,t) + R(x,t) \Big\} dx.$$

The following assumptions are taken into the account to construct the desired mathematical model:

- Each newborn is susceptible i.e., having the capability of getting infection.
- The population in I_S and I_A are capable to transmit the infection.
- Vaccination is not permanent. The vaccinated individuals can wane vaccine immunity and become susceptible again.

The desired nonlinear spatio-temporal COVID-19 epidemic model is presented as follows:

$$\begin{aligned}
\frac{\partial S}{\partial t} &= D_S \frac{\partial^2 S}{\partial x^2} + b + \psi_V V - \tfrac{\beta(I_S + \beta_1 I_A)S}{N} - (\mu + \omega_V)S, \\
\frac{\partial E}{\partial t} &= D_E \frac{\partial^2 E}{\partial x^2} + \tfrac{\beta(I_S + \beta_1 I_A)S}{N} - (\kappa + \mu)E, \\
\frac{\partial I_S}{\partial t} &= D_{I_S} \frac{\partial^2 I_S}{\partial x^2} + (1 - \eta)\kappa E - (\mu + \mu_1 + \gamma_1)I_S, \\
\frac{\partial I_A}{\partial t} &= D_{I_A} \frac{\partial^2 I_A}{\partial x^2} + \eta\kappa E - (\mu + \gamma_2)I_A, \\
\frac{\partial V}{\partial t} &= D_V \frac{\partial^2 V}{\partial x^2} + \omega_V S - (\psi_V + \mu)V, \\
\frac{\partial R}{\partial t} &= D_R \frac{\partial^2 R}{\partial x^2} + \gamma_1 I_S + \gamma_2 I_A - \mu R,
\end{aligned} \tag{2.1}$$

subjected to non-negative initial conditions (ICs):

$$\begin{cases} S(0,x) &= S_0 \exp\left(-\left(\frac{x}{0.7}\right)^2\right), \\ E(0,x) &= E_0 \exp\left(-\left(\frac{x}{0.8}\right)^2\right), \\ I_S(0,x) &= I_{S0} \exp\left(-\left(\frac{x}{0.5}\right)^2\right), \\ I_A(0,x) &= I_{A0} \exp\left(-\left(\frac{x}{0.2}\right)^2\right), \\ V(0,x) &= 0, \\ R(0,x) &= 0, \end{cases} \tag{2.2}$$

where $S(0,x) = S_0 \geq 0, E(0,x) = E_0 \geq 0, I_S(0,x) = I_{S0} \geq 0, I_A(0,x) = I_{A0} \geq 0, V(0,x) = R(0,x) = 0$ and $x \in [-2,2]$ is the computational domain for the proposed model (2.1). The biological description of embedded parameters is shown in the Table 2. Further, $D_S, D_E, D_{I_S}, D_{I_A}, D_V$ and D_R are the coefficients of diffusivity for the respective population groups. Furthermore, no flux boundary conditions are being imposed for the proposed model given by:

$$\begin{cases} S_x(-2,t) &= E_x(-2,t) = I_{Sx}(-2,t) = I_{Ax}(-2,t) = V_x(-2,t) = R_x(-2,t) = 0, \\ S_x(2,t) &= E_x(2,t) = I_{Sx}(2,t) = I_{Ax}(2,t) = V_x(2,t) = R_x(2,t) = 0. \end{cases} \tag{2.3}$$

Table 1. Model (2.1) variables.

State variables	Definition
S	Susceptible individuals
E	Exposed individuals
I_S	Symptomatically Infected individuals
I_A	Asymptomatically Infected individuals
V	Vaccinated population
R	Recovered individuals

Table 2. Physical/biological description of the model embedded parameters. The parameters are estimated from reported COVID-19 cases in Pakistan [19].

Parameter	Physical/bilogical description	value (per day)
b	birth rate	8939
μ	natural mortality rate	$1/(67.7 \times 365)$
μ_1	death rate caused due to infection	0.022
γ_1	recovery/removal rate of infected person with symptoms	0.4958
γ_2	recovery/removal rate of infected person with no clinical symptoms	0.1110
β	infection transmission rate	0.6022
β_1	infection transmission probability relative person with no clinical symptoms	0.7459
κ	incubation period	0.5171
η	proportion of exposed people join I_A class	0.8833
ω_V	vaccine rate	0.0313
ψ_V	vaccine wanning/loss of immunity	0.0233

3. Theoretical analysis of model

In the current section, we establish some of the important theoretical analyses of the proposed COVID-19 reaction-diffusion model (2.1). The well-known threshold parameter of the epidemiological model is derived. Moreover, the disease free and endemic equilibria of model (2.1) are computed. In addition, the stability results of the model are accomplished.

3.1. Well-posedness of model (2.1)

The well-posedness of partial differential equations (PDEs) with some initial and boundary conditions is important to verify in order to claim the existence and uniqueness of its solution. For this purpose, the semi-group theory approach can be utilized to check when a problem is well-posed. To proceeds with this analysis, a Banach space $X = C(\Xi; \mathbb{R})$ is considered, which is a space of real-valued continuous function Υ define on Ξ and X_+ is a positive cone. The space is combined with norm $\|\Upsilon\|_X = \sup_{x\in\Xi} |\Upsilon(x)|$. Assume that $\mathcal{A}_\xi$ is a linear operator defined by

$$\mathcal{A}_\xi(\Upsilon) = \alpha_\xi \Delta \Upsilon,$$

where ξ represent the state variables S, E, I_S, I_V, V, R and Δ is the second order differential operator $\frac{\partial^2}{\partial x^2}$. Further,

$$D(\mathcal{A}_\xi) = \left\{ \Upsilon \in X : \Delta\Upsilon \in X, \frac{\partial \Upsilon}{\partial x} = 0 \text{ on } \delta\Xi \right\}.$$

After utilizing the well-known facts regarding the operator $\mathcal{A}_\xi$, i.e., $\mathcal{A}_\xi$ is an infinitesimal generator of a strongly continuous semi-group $\{e^{t\mathcal{A}_\xi} : t \geq 0\}$ of linear operators in X [20]. On other hand the operator,

$$\mathcal{A}(\phi_1,\phi_2,\phi_3,\phi_4,\phi_5,,\phi_6)=\begin{pmatrix}\mathcal{A}_\xi(\phi_1)\\ \mathcal{A}_\xi(\phi_2)\\ \mathcal{A}_\xi(\phi_3)\\ \mathcal{A}_\xi(\phi_4)\\ \mathcal{A}_\xi(\phi_5)\\ \mathcal{A}_\xi(\phi_6)\end{pmatrix}, D(\mathcal{A})=D(\mathcal{A}_\xi)\times D(\mathcal{A}_\xi), \tag{3.1}$$

is an infinitesimal generator of a strongly continuous semi-group $\{e^{t\mathcal{A}} : t \geq 0\}$ of linear operators in $Y = X^6$ [20], where Y is a Banach space with norm define by,

$$\|(\phi_1,\phi_2,\phi_3,\phi_4,\phi_5,\phi_6)\|_Y=\|\phi_1\|_Y+\|\phi_2\|_Y+\|\phi_3\|_Y+\|\phi_4\|_Y+\|\phi_5\|_Y+\|\phi_6\|_Y$$

and $Y_+ = X^6_+ \subset Y$ be a positive cone in Y. Let F be a nonlinear operator define on Y as:

$$F(\phi_1,\phi_2,\phi_3,\phi_4,\phi_5,\phi_6)=\begin{pmatrix}b-\beta(\phi_3+\beta_1\phi_4)\dfrac{\phi_1}{N}+\psi_V\phi_5-(\mu+\omega_V)\phi_1\\ \beta(\phi_3+\beta_1\phi_4)\dfrac{\phi_1}{N}-(\mu+\kappa)\phi_2\\ (1-\eta)\kappa\phi_2-(\mu+\mu_1+\gamma_1)\phi_3\\ \eta\kappa\phi_2-(\mu+\gamma_2)\phi_4\\ \omega\phi_1-(\mu+\psi_V)\phi_5\\ \gamma_1\phi_3+\gamma_2\phi_4-\mu\phi_6\end{pmatrix},$$

for $(\phi_1,\phi_2,\phi_3,\phi_4,\phi_5,\phi_6) \in Y_+$. Thus model (2.1) can be expressed in compact form as:

$$\frac{d}{dt}u(t)=\mathcal{A}u(t)+F(u(t)), \tag{3.2}$$

where

$$u(t)=\begin{pmatrix}S(.,t)\\ E(.,t)\\ I_S(.,t)\\ I_A(.,t)\\ V(.,t)\\ R(.,t)\end{pmatrix}, \text{ and } u(0)=\begin{pmatrix}S_0(.)\\ E_0(.)\\ I_{S0}(.)\\ I_{A0}(.)\\ V_0(.)\\ R_0(.)\end{pmatrix}.$$

Clearly, F is Lipschitz continuous on Y_+. Since the following inequality holds,

$$\|F(x)-F(y)\|\leq L\|x-y\| \text{ for all } x,y\in Y_+,$$

where $L = \mu + \mu_1 + 2(\psi_V + \kappa + \gamma_1 + \gamma_2 + \omega_V)$. Hence, by Theorem 3.3.3 in [21], the following result is concluded.

Proposition 3.1. *Assume that $\mathcal{A}$ be an operator define by* (3.1) *and for each $u_0 = (S_0, E_0, I_{S0}, I_{S0}, V_0, R_0)^T \in Y_+$ there exist a unique continuously differentiable solution $u(t)$ of* (3.2) *define on some maximum interval of existence* $[0, \tau]$ *such that*

$$u(t)=u_0e^{t\mathcal{A}}+\int_0^t e^{(t-\zeta)\mathcal{A}}F(u(\zeta))d\zeta.$$

3.2. Positivity and boundedness

To show that the solution of model (2.1) is non-negative, we follow the lemma provided in [22–24].

Lemma 3.2. *Assume that* $u \in C(\bar{\Xi} \times [0,\tau)) \bigcap C^{2,1}(\Xi \times (0,\tau))$ *satisfy*

$$\left.\begin{aligned} &\frac{\partial}{\partial t}u(x,t) - D\Delta u(x,t) \geq k(x,t)u(x,t), && x \in \Xi, t \in [0,\tau) \\ &\frac{\partial}{\partial t}u(x,t) \geq 0, && x \in \delta\Xi, t \in [0,\tau) \\ &u(x,0) \geq 0, && x \in \bar{\Xi}, t \in [0,\tau) \end{aligned}\right\}$$

where $k(x,t) \in C(\bar{\Xi} \times [0,\tau))$. *Then* $u(x,t) \geq 0$ *0n* $\bar{\Xi} \times [0,\tau)$ *and* $u(x,t) > 0$ *or* $u(x,t) \equiv 0$ *in* $\Xi \times [0,\tau)$

In view of the above Lemma 3.2, the following result is obtained.

Proposition 3.3. *The solution* $(S(.,t), E(.,t), I_S(.,t), I_A(.,t), V(.,t), R(.,t))$ *of model* (2.1) *is non-negative on* $\Xi \times [0,\tau)$ *provided that the initial condition* $(S(.), E(.), I_S(.), I_A(.), V(.), R(.))$ *is non-negative.*

Proof. Suppose $\mathcal{K}(x,t) = \beta(I_S(x,t) + \beta_1 I_A(x,t))\frac{1}{N} + (\mu + \omega_V)$. Then from first equation of model (2.1)

$$\left.\begin{aligned} &\frac{\partial}{\partial t}S(x,t) - D_S\frac{\partial^2}{\partial x^2}S(x,t) > -\mathcal{K}(x,t)S(x,t), && x \in \Xi, t \in [0,\tau) \\ &\frac{\partial}{\partial x}S(x,t) = 0, && x \in \delta\Xi, t \in [0,\tau) \\ &S(x,0) > 0, && x \in \Xi, t \in [0,\tau) \end{aligned}\right\} \tag{3.3}$$

Clearly, (3.3) fulfill the conditions of Lemma 3.2. So, by direct application of Lemma 3.2 $S(x,t) \geq 0$ on $\Xi \times [0,\tau)$. The non-negativity of the rest of state variables $E(x,t)$, $I_S(x,t)$, $I_A(x,t)$, $V(x,t)$ and $R(x,t)$ can be prove in similar manner.

Next, the boundedness of solution of model (2.1) is demonstrated in order to prove the time existence of global solution. For this the following result is derived.

Theorem 3.4. *The solution* $(S(.,t), E(.,t), I_S(.,t), I_A(.,t), V(.,t), R(.,t))$ *of model* (2.1) *is bounded for all* $t \geq 0$.

Proof. By sum up all equations of model (2.1), we obtained

$$\begin{aligned} &\frac{\partial S(x,t)}{\partial t} + \frac{\partial E(x,t)}{\partial t} + \frac{\partial I_S(x,t)}{\partial t} + \frac{\partial I_A(x,t)}{\partial t} + \frac{\partial V(x,t)}{\partial t} + \frac{\partial R(x,t)}{\partial t} \\ &\quad = D_S\frac{\partial^2 S(x,t)}{\partial x^2} + D_E\frac{\partial^2 E(x,t)}{\partial x^2} + D_{I_S}\frac{\partial^2 I_S(x,t)}{\partial x^2} + D_{I_A}\frac{\partial^2 I_A(x,t)}{\partial x^2} + D_V\frac{\partial^2 V(x,t)}{\partial x^2} + D_R\frac{\partial^2 R(x,t)}{\partial x^2} \\ &\quad + b - \mu(S(x,t) + E(x,t) + I_S(x,t) + I_A(x,t) + V(x,t) + R(x,t)) - \mu_1 I_S(x,t). \end{aligned}$$

Integrating over $\Xi = [-2, 2]$ yields to,

$$\begin{aligned}\int_{\Xi}\Big\{\frac{\partial S(x,t)}{\partial t}+\frac{\partial E(x,t)}{\partial t}+\frac{\partial I_S(x,t)}{\partial t}+\frac{\partial I_A(x,t)}{\partial t}+\frac{\partial V(x,t)}{\partial t}+\frac{\partial R(x,t)}{\partial t}\Big\}dx\\ =\int_{\Xi}\Big\{D_S\frac{\partial^2 S(x,t)}{\partial x^2}+D_E\frac{\partial^2 E(x,t)}{\partial x^2}+D_{I_S}\frac{\partial^2 I_S(x,t)}{\partial x^2}+D_{I_A}\frac{\partial^2 I_A(x,t)}{\partial x^2}+D_V\frac{\partial^2 V(x,t)}{\partial x^2}\\ +D_R\frac{\partial^2 R(x,t)}{\partial x^2}\Big\}dx+\int_{\Xi}\Big\{b-\mu(S(x,t)+E(x,t)+I_S(x,t)+I_A(x,t)+V(x,t)\\ +R(x,t))-\mu_1 I_S(x,t)\Big\}dx.\end{aligned}$$

By utilizing the no flux boundary conditions imposed to the problem we have

$$\int_{\Xi}\Big\{D_S\frac{\partial^2 S(x,t)}{\partial x^2}+D_E\frac{\partial^2 E(x,t)}{\partial x^2}+D_{I_S}\frac{\partial^2 I_S(x,t)}{\partial x^2}+D_{I_A}\frac{\partial^2 I_A(x,t)}{\partial x^2}+D_V\frac{\partial^2 V(x,t)}{\partial x^2}+D_R\frac{\partial^2 R(x,t)}{\partial x^2}\Big\}dx=0.$$

Therefore,

$$\begin{aligned}\int_{\Xi}\Big\{\frac{\partial S(x,t)}{\partial t}+\frac{\partial E(x,t)}{\partial t}+\frac{\partial I_S(x,t)}{\partial t}+\frac{\partial I_A(x,t)}{\partial t}+\frac{\partial V(x,t)}{\partial t}+\frac{\partial R(x,t)}{\partial t}\Big\}dx\\ =b|\Xi|-\mu\int_{\Xi}\Big\{S(x,t)+E(x,t)+I_S(x,t)+I_A(x,t)+V(x,t)+R(x,t)\Big\}dx\\ -\mu_1\int_{\Xi}I_S(x,t)dx\\ \le b|\Xi|-\mu\int_{\Xi}\Big\{S(x,t)+E(x,t)+I_S(x,t)+I_A(x,t)+V(x,t)+R(x,t)\Big\}dx\\ =b|\Xi|-\mu\mathcal{N}(t),\\ \frac{d}{dt}\mathcal{N}(t)\le b|\Xi|-\mu\mathcal{N}(t).\end{aligned}$$

It follows that

$$0\ge\mathcal{N}(t)\le\frac{b|\Xi|}{\mu}+\mathcal{N}(0)\exp(-\mu t).$$

Thus,

$$\lim_{t\to+\infty}\mathcal{N}(t)\le\frac{b|\Xi|}{\mu}.$$

Invariant region

The transmission dynamics of the problem is studied in the biological feasible region given by,

$$\Delta\subset\mathbf{R}_+^6,$$

where,

$$\Delta=\Big\{(S(x,t),E(x,t),I_S(x,t),I_A(x,t),V(x,t),R(x,t))\in\mathbf{R}_+^6:\mathcal{N}(t)\le\frac{\Theta|\Xi|}{\mu}\Big\}.$$

3.3. Steady-state of the model

The proposed spatio-temporal vaccine model (2.1) has two steady-states. The disease free steady-state is

$$\mathcal{E}_0 = \left(S^0, 0, 0, 0, V_0, 0\right) = \left(\frac{b}{\mu}, 0, 0, 0, \frac{b\omega_V}{\psi_V\omega_V - (\mu+\omega_V)(\psi_V+\mu)}, 0\right).$$

The endemic equilibrium is stated as follows: $\mathcal{E}_1(S^{***}, E^{***}, I_S^{***}, I_A^{***}, V^{***}, R^{***})$ with

$$\begin{cases} S^{***} = \frac{bc_4}{\lambda^{***}c_4 + c_0c_4 - \psi_V\omega_V}, \\ E^{***}_{=} \frac{b\lambda^{***}c_4}{c_1(\lambda^{***}c_4 + c_0c_4 - \psi_V\omega_V)}, \\ I_S^{***} = \frac{B\kappa\lambda^{***}c_4(1-\eta)}{c_2c_1(\lambda^{***}c_4 + c_0c_4 - \psi_V\omega_V)}, \\ I_A^{***} = \frac{b\kappa\lambda^{***}c_4\eta}{c_1c_3(\lambda^{***}c_4 + c_0c_4 - \psi_V\omega_V)}, \\ V^{***} = \frac{b\omega_V}{\lambda^{***}c_4 + c_0c_4 - \psi_V\omega_V}, \\ R^{***} = \frac{b\kappa\lambda^{***}c_4(c_3(1-\eta)\gamma_1 + c_2\eta\gamma_2)}{c_1c_2c_3d(\lambda^{***}c_4 + c_0c_4 - \psi_V\omega_V)}, \end{cases} \tag{3.4}$$

where,

$$c_0 = (\mu+\omega_V), c_1 = (\kappa+\mu), c_2 = (\mu+\mu_1+\gamma_1), c_3 = (\mu+\gamma_2), c_4 = (\psi_V+\mu).$$

Substituting values from (3.4) into the following force of infection:

$$\lambda^{\star\star\star} = \frac{\beta({I_S}^{\star\star\star} + \beta_1 I_A^{\star\star\star})}{N^{\star\star\star}}. \tag{3.5}$$

After some manipulations, the non-zero equilibria of the model satisfies the following equation

$$C_0\lambda^{\star\star\star} + C_1 = 0, \tag{3.6}$$

with the coefficients

$$\begin{aligned} C_0 &= c_4\{\kappa c_3(1-\eta)(\gamma_1+\mu) + c_2(c_3\mu + \kappa\eta(\mu+\gamma_2))\}, \\ C_1 &= \mu c_1c_2c_3(c_4+\omega_V)(1-\mathcal{R}_0). \end{aligned}$$

The basic reproduction number $\mathcal{R}_0$ is the epidemiological threshold parameter called the basic reproductive number. By utilizing the next generation technique $\mathcal{R}_0$ is computed as fallow:

$$\mathcal{R}_0 = \frac{\beta\kappa(\psi_V+\mu)(\eta\beta_1(\mu+\mu_1+\gamma_1) + c_3(1-\eta))}{(\mu+\mu_1+\gamma_1)(\kappa+\mu)(\mu+\gamma_2)((\psi_V+\mu+\omega_V)}. \tag{3.7}$$

3.4. Stability of the model equilibria

In this subsection, we provide the stability analysis of the spatio-temporal COVID-19 model (2.1). In order to investigate the local stability of the model at $\mathcal{E}_0$, we follow the Fourier series expansion technique discussed in [15]. The variational matrix obtained after linearizing the spatio-temporal COVID-19 model (2.1) is given as follows:

$$\mathbf{V} = \begin{pmatrix} -b_{11} & 0 & -\frac{\beta c_4}{c_4+\omega_v} & -\frac{\beta c_4 \beta_1}{c_4+\omega_V} & \psi_V & 0 \\ 0 & -b_{22} & \frac{\beta c_4}{c_4+\omega_v} & \frac{\beta c_4 \beta_1}{c_4+\omega_V} & 0 & 0 \\ 0 & (1-\eta)\kappa & -b_{33} & 0 & 0 & 0 \\ 0 & \eta\kappa & 0 & -b_{44} & 0 & 0 \\ \omega_V & 0 & 0 & 0 & -b_{55} & 0 \\ 0 & 0 & \gamma_1 & \gamma_2 & 0 & -b_{66} \end{pmatrix}, \tag{3.8}$$

where,

$$\begin{aligned} b_{11} &= c_0 + D_S k^2,\ b_{22} = c_1 + D_E k^2,\ b_{33} = c_2 + D_{I_S} k^2,\ b_{44} = c_3 + D_{I_A} k^2, \\ b_{55} &= c_4 + D_V k^2,\ b_{66} = \mu + D_R k^2. \end{aligned} \tag{3.9}$$

The corresponding characteristic equation of the variational matrix $\mathbf{V}$ is obtained as:

$$(\lambda + \mu + D_R k^2)(\lambda^5 + a_1\lambda^4 + a_2\lambda^3 + a_3\lambda^2 + a_4\lambda + a_5) = 0. \tag{3.10}$$

The eigenvalue $-(\mu + D_S k^2)$ has negative real part while the following coefficients of (3.10) are obtained

$$\begin{aligned} a_1 &= b_{11} + b_{22} + b_{33} + b_{44} + b_{55}, \\ a_2 &= b_{22}b_{33}(1 - \frac{\beta c_4(1-\eta)\kappa}{b_{22}b_{33}(c_4+\omega_V)}) + b_{22}b_{44}(1 - \frac{\beta\beta_1 c_4\kappa\eta}{b_{22}b_{44}(c_4+\omega_V)}) + b_{11}b_{22} + b_{11}b_{33} + b_{11}b_{44} + b_{33}b_{44} \\ &\quad + b_{11}b_{55} + b_{22}b_{55} + b_{33}b_{55} + b_{44}b_{55} - \psi_V\omega_V, \\ a_3 &= b_{22}b_{33}\left(b_{11}+b_{44}+b_{55}\right)\left(1 - \frac{\beta c_4(1-\eta)\kappa}{b_{22}b_{33}\left(c_4+\omega_V\right)}\right) + b_{22}b_{44}\left(b_{11}+b_{33}+b_{55}\right)\left(1 - \frac{\beta\beta_1 c_4\kappa\eta}{b_{22}b_{44}\left(c_4+\omega_V\right)}\right) - \\ &\quad \left(b_{22}+b_{33}+b_{44}\right)\psi\omega + b_{11}b_{33}b_{44} + b_{11}b_{55}b_{44} + b_{33}b_{55}b_{44} + b_{11}b_{22}b_{55} + b_{11}b_{33}b_{55}, \\ a_4 &= b_{22}b_{33}\left(b_{11}+b_{44}+b_{55}\right)\left(1 - \frac{\beta c_4(1-\eta)\kappa}{b_{22}b_{33}\left(c_4+\omega_V\right)}\right) + b_{22}b_{44}\left(b_{11}+b_{33}+b_{55}\right)\left(1 - \frac{\beta\beta_1 c_4\kappa\nu}{b_{22}b_{44}\left(c_4+\omega_V\right)}\right) - \\ &\quad \left(b_{22}+b_{33}+b_{44}\right)\psi_V\omega_V + b_{11}b_{33}b_{44} + b_{11}b_{55}b_{44} + b_{33}b_{55}b_{44} + b_{11}b_{22}b_{55} + b_{11}b_{33}b_{55}, \\ a_5 &= b_{22}b_{33}b_{44}\left(b_{11}b_{55} - \psi_V\omega_V\right)\left(1 - \frac{\beta c_4(1-\eta)\kappa}{b_{22}b_{33}\left(c_4+\omega_V\right)} - \frac{\beta\beta_1 c_4\kappa\eta}{b_{22}b_{44}\left(c_4+\omega_V\right)}\right). \end{aligned}$$

After substituting values from (3.9), it can be shown that $a_i > 0$ for $i = 1, 2, ..., 5$ under the condition $\mathcal{R}_0 < 1$. Furthermore, after some manipulation, the Routh-Hurwitz criteria for characteristic polynomial (3.10) arrived when $\mathcal{R}_0 < 1$. Thus, the spatio-temporal COVID-19 (2.1) is locally asymptotically at $\mathcal{E}_0$ whenever, $\mathcal{R}_0 < 1$.

Moreover, to inveterate the global asymptotical stability of the spatio-temporal model (2.1) at $\mathcal{E}_0$, the well-known Lyapunov function approach is implemented. The subsequent theorem yield the desired result.

Theorem 3.5. *If $\mathcal{R}_0 \leq 1$, the equilibrium point $\mathcal{E}_0$ of model* (2.1) *is globally asymptotically stable.*

Proof. To prove the result, consider Lyapunov functional as follows:

$$\mathcal{F}(t) = \int_\Xi \left\{ g_1 E(x,t) + \int_{t_0}^{g_1(\mu+\kappa)t} E\left(x, \frac{\sigma}{g_1(\mu+\kappa)}\right) d\sigma + \int_{(\mu+\kappa)t}^{\tau} E\left(x, \frac{\sigma}{\mu+\kappa}\right) d\sigma \right\} dx + g_2 \int_\Xi I(x,t)dx + g_3 \int_\Xi I_A(x,t)dx,$$

where $g_1 = \dfrac{\mu+\psi_V}{\mu+\psi_V+\omega_V}$, $g_2 = \dfrac{\beta g_1}{(\mu+\mu_1+\gamma_1)(\mu+\gamma_2)}$, $g_2 = \dfrac{\beta\beta_1 g_1}{\mu+\gamma_2}$ and τ is the maximum time.

Then, the time derivative $\mathcal{F}(t)$ is given by

$$\begin{aligned}\frac{d}{dt}\mathcal{F}(t) = &\int_\Xi \left\{ g_1 D_E \frac{\partial^2 E(x,t)}{\partial x^2} + g_1\beta(I_S(x,t) + \kappa I_A(x,t))\frac{S(x,t)}{N(x,t)} \right\} dx - (\mu+\kappa)\int_\Xi E(x,t)\,dx \\ &+ g_2 \int_\Omega \left\{ D_{I_S} \frac{\partial^2 I_S(x,t)}{\partial x^2} + (1-\eta)\kappa E(x,t) - (\mu+\mu_1+\gamma_1) I_S(x,t) \right\} dx \\ &+ g_3 \int_\Xi \left\{ D_{I_A} \frac{\partial^2 I_A(x,t)}{\partial x^2} + \eta\kappa E(x,t) - (\mu+\gamma_2) I_A(x,t) \right\} dx\end{aligned}$$

By utilizing the no flux boundary conditions implies,

$$\int_\Xi \left\{ g_1 D_E \frac{\partial^2 E(x,t)}{\partial x^2} + g_2 D_{I_S} \frac{\partial^2 I_S(x,t)}{\partial x^2} + g_3 D_{I_A} \frac{\partial^2 I_A(x,t)}{\partial x^2} \right\} dx = 0.$$

Since,

$$\mathcal{S}(x,t) \leq \mathcal{N}(x,t) \text{ for all } t \geq 0, x \in \Xi.$$

Therefore,

$$\begin{aligned}\frac{d}{dt}\mathcal{F}(t) &\leq \int_\Xi \left(\left\{ g_2(1-\eta)\kappa + g_3\eta\kappa - (\mu+\kappa) \right\} E(x,t) + \left\{ g_1\beta - g_2(\mu+\mu_1+\gamma_1) \right\} I_S(x,t) \right) dx, \\ &= \int_\Xi \left\{ g_1\beta\beta_1\kappa - g_3(\mu+\gamma_2) \right\} I_A(x,t)dx \\ &\leq (\mu+\kappa)\int_\Xi \left\{ g_1 \left(\frac{\beta\kappa(1-\eta) + \beta\beta_1(\mu+\mu_1+\gamma_1)}{(\mu+\kappa)(\mu+\mu_1+\gamma_1)(\mu+\gamma_2)} \right) - 1 \right\} E(x,t)dx, \\ &= (\mu+\kappa)(\mathcal{R}_0 - 1)\int_\Xi E(x,t)dx.\end{aligned}$$

It is clear that $\frac{d}{dt}\mathcal{F}(t) \leq 0$ for all $t \geq 0$ and $x \in \Xi$ if and only if $\mathcal{R}_0 \leq 1$. Moreover $\frac{d}{dt}\mathcal{F}(t) = 0$ whenever, $E(x,t) \to 0$, for all $t \geq 0$ and $x \in \Xi$. It follows from the well-known LaSalle's invariance principle presented in [25], that the equilibrium $\mathcal{E}_0$ of spatio-temporal model (2.1) is globally asymptotically stable if $\mathcal{R}_0 \leq 1$.

4. Numerical method and simulation

This section presents the numerical scheme of the proposed spatio-temporal COVID-19 model (2.1). The operator-splitting finite difference approximation technique is utilized for the numerical solution and is described in detail as follows:

4.1. Numerical scheme

The operator splitting approach is a well-known and efficient numerical technique. It has been applied to solve nonlinear partial differential equations arising from nonlinear and complex problems. In this scheme, we split the differential operator into sub-operators and split the problems under consideration for solution into sub-problems, where each of these problems correspond to a particular physical phenomenon. Further, the operator-splitting technique is implemented to solve the proposed reaction-diffusion epidemic model (2.1). Each differential equation in the model (2.1) denotes the physical process consisting of two individual processes: the population with different disease status interacting with each other and diffusing spatially in one direction, required different time steps. It is therefore important to split the time operator and shift model (2.1) into two sub-systems: The resulting non-linear reaction system used for time step t_0 to $\frac{1}{2}dt$ is,

$$\begin{cases} \frac{1}{2}\frac{\partial S}{\partial t} &= b + \psi_V V - \frac{\beta(I_S+\beta_1 I_A)S}{N} - (\mu+\omega_V)S, \\ \frac{1}{2}\frac{\partial E}{\partial t} &= \frac{\beta(I_S+\beta_1 I_A)S}{N} - (\kappa+\mu)E, \\ \frac{1}{2}\frac{\partial I_S}{\partial t} &= (1-\eta)\kappa E - (\mu+\mu_1+\gamma_1)I_S, \\ \frac{1}{2}\frac{\partial I_A}{\partial t} &= \eta\kappa E - (\mu+\gamma_2)I_A, \\ \frac{1}{2}\frac{\partial V}{\partial t} &= \omega_V S - (\psi_V+\mu)V, \\ \frac{1}{2}\frac{\partial R}{\partial t} &= \gamma_1 I_S + \gamma_2 I_A - \mu R, \end{cases} \tag{4.1}$$

and the linear diffusion system used for time step $\frac{1}{2}dt$ to t^n is,

$$\begin{cases} \frac{1}{2}\frac{\partial S}{\partial t} &= D_S \frac{\partial^2 S}{\partial x^2}, \\ \frac{1}{2}\frac{\partial E}{\partial t} &= D_E \frac{\partial^2 E}{\partial x^2}, \\ \frac{1}{2}\frac{\partial I_S}{\partial t} &= D_{I_S} \frac{\partial^2 I_S}{\partial x^2}, \\ \frac{1}{2}\frac{\partial I_A}{\partial t} &= D_{I_A} \frac{\partial^2 I_A}{\partial x^2}, \\ \frac{1}{2}\frac{\partial V}{\partial t} &= D_V \frac{\partial^2 V}{\partial x^2}, \\ \frac{1}{2}\frac{\partial R}{\partial t} &= D_R \frac{\partial^2 R}{\partial x^2}, \end{cases} \tag{4.2}$$

using conventional finite difference approximations, the first order time derivative in (4.1) and (4.2) is approximated by first order-forward difference,

$$\frac{\partial \xi_j^n}{\partial t} = \frac{\xi_j^{n+1} - \xi_j^n}{dt}, \tag{4.3}$$

while the second order spatial derivative in (4.2) is approximated by second order central finite difference given by,

$$\frac{\partial^2 \xi_j^n}{\partial x^2} = \frac{\xi_{j-1}^n - \xi_j^n + \xi_{j+1}^n}{dx}, \tag{4.4}$$

where ξ represent each of the variables S, E, I_S, I_A, V and R. The sub-systems (4.1) and (4.2) in iterative form can be written as fallow:

$$\begin{cases} S_j^{n+\frac{1}{2}} &= S_j^n + dt\left(b + \psi_V V_j^n - \frac{\beta(I_{S_j}^n + \beta_1 I_{A_j}^n)S_j^n}{N_j^n} - (\mu + \omega_V)S_j^n\right), \\ E_j^{n+\frac{1}{2}} &= E_j^n + dt\left(\frac{\beta(I_{S_j}^n + \beta_1 I_{A_j}^n)S_j^n}{N_j^n} - (\kappa + \mu)E_j^n\right), \\ {I_S}_j^{n+\frac{1}{2}} &= {I_S}_j^n + dt\left(\kappa(1-\eta)E_j^n - (\mu + \mu_1 + \gamma_1){I_S}_j^n\right), \\ {I_A}_j^{n+\frac{1}{2}} &= {I_A}_j^n + dt\left(\kappa\eta E_j^n - (\mu + \gamma_2){I_A}_j^n\right), \\ V_j^{n+\frac{1}{2}} &= V_j^n + dt\left(\omega {S_S}_j^n - (\phi_V + \mu)V_j^n\right), \\ R_j^{n+\frac{1}{2}} &= R_j^n + dt\left(\gamma_1 {I_S}_j^n + \gamma_2 {I_A}_j^n - \mu R_j^n\right), \end{cases} \tag{4.5}$$

and

$$\begin{cases} S_j^{n+1} &= S_j^{n+\frac{1}{2}} + D_S \dfrac{dt}{dx^2}\left(S_{j-1}^{n+\frac{1}{2}} - 2S_j^{n+\frac{1}{2}} + S_{j+1}^{n+\frac{1}{2}}\right), \\ E_j^{n+1} &= E_j^{n+\frac{1}{2}} + D_E \dfrac{dt}{dx^2}\left(E_{j-1}^{n+\frac{1}{2}} - 2E_j^{n+\frac{1}{2}} + E_{j+1}^{n+\frac{1}{2}}\right), \\ {I_S}_j^{n} &= {I_S}_j^{n+\frac{1}{2}} + D_{I_S} \dfrac{dt}{dx^2}\left({I_S}_{j-1}^{n+\frac{1}{2}} - 2{I_S}_j^{n+\frac{1}{2}} + {I_S}_{j+1}^{n+\frac{1}{2}}\right), \\ {I_A}_j^{n} &= {I_A}_j^{n+\frac{1}{2}} + D_{I_A} \dfrac{dt}{dx^2}\left({I_A}_{j-1}^{n+\frac{1}{2}} - 2{I_A}_j^{n+\frac{1}{2}} + {I_A}_{j+1}^{n+\frac{1}{2}}\right), \\ V_j^{n} &= V_j^{n+\frac{1}{2}} + D_V \dfrac{dt}{dx^2}\left(V_{j-1}^{n+\frac{1}{2}} - 2V_j^{n+\frac{1}{2}} + V_{j+1}^{n+\frac{1}{2}}\right), \\ R_j^{n+1} &= R_j^{n+\frac{1}{2}} + D_R \dfrac{dt}{dx^2}\left(R_{j-1}^{n+\frac{1}{2}} - 2R_j^{n+\frac{1}{2}} + R_{j+1}^{n+\frac{1}{2}}\right), \end{cases} \tag{4.6}$$

4.2. Simulation and discussions

In this section, numerical simulations of the proposed reaction-diffusion epidemic model (2.1) is performed using the iterative scheme derived in (4.5) and (4.6). The purpose of the model simulation is to analyze the impact of diffusion phenomena under several control strategies. Model (2.1) is simulated in two ways: with and without diffusion in parallel with other control measures such as, the effective contact rate β, the transmissibility of infection relative to asymptomatically infected individuals β_1, the vaccine waning rate ψ_V and the effective vaccination rate ω_V. The simulation is performed based on initial conditions (2.2) and estimated parameters given in Tabe 2, while the diffusion coefficients are assumed as $D_S = 0.00005, D_E = 0.0005, D_{I_S} = 0.0001, D_{I_A} = 0.001, D_V = 0.0001, D_R = 0$ so that the quantity

$$D_\xi \frac{dt}{dx^2} \leq 0.5, \tag{4.7}$$

where ξ represents each of the state variables. In order to perform simulation, the spatial step is taken as $dx = 0.06$ and the time step $dt = 0.02$ days based on Von Neumann stability criteria [26]. Figure 1 demonstrate in detail the dynamics of exposed, symptomatically and asymptomatically infected individuals, with and without diffusion using the baseline values of the model (2.1) embedded parameters. From the corresponding plots, it is observed that the number of infected individuals in all categories reduces significantly, in the case of diffusion as compared to without diffusion. Physically, it means that restricting public gathering plays an important role in reducing the transmission of infection. In the subsequent sections, we present the impact of different control interventions as mentioned before on the dynamics of exposed, symptomatically and asymptomatically infected individuals in case of diffusion and without diffusion. In Table 3, we compare the results of the present technique with fully explicit Euler scheme in terms of CPU time.

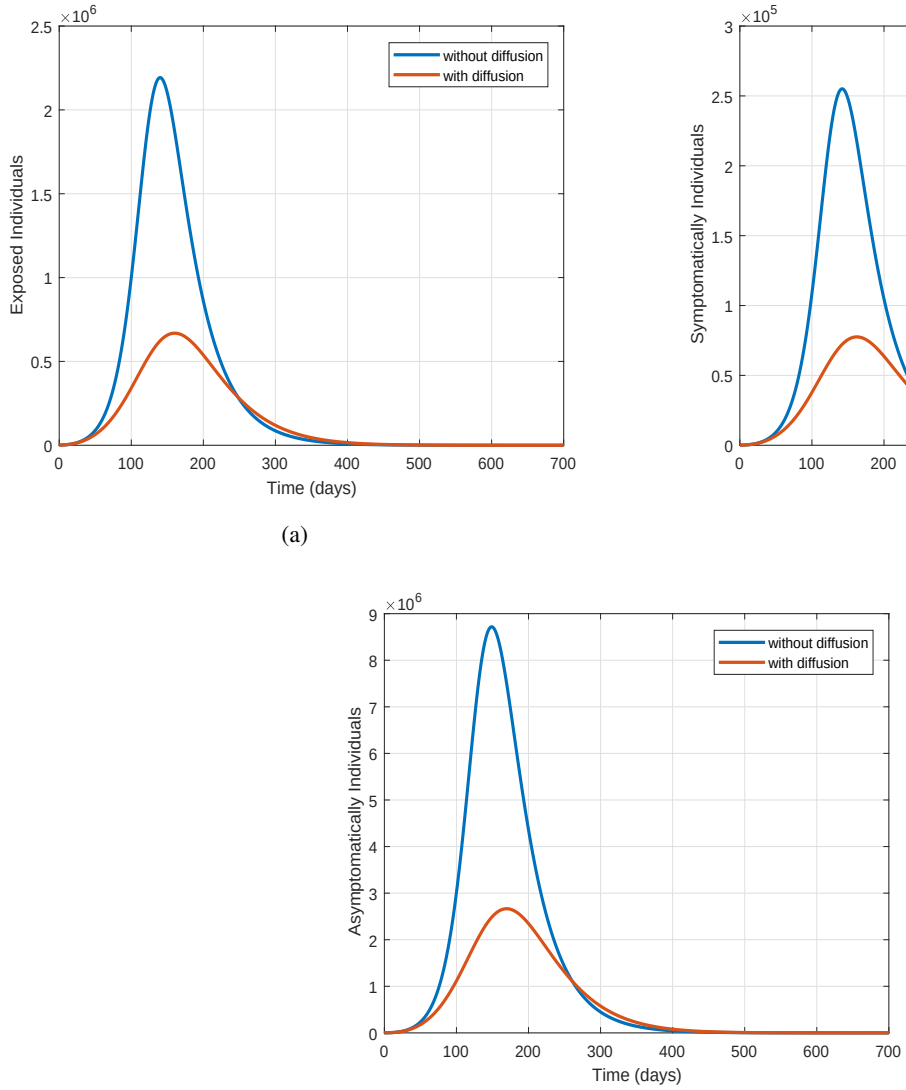

Figure 1. Dynamics of exposed, symptomatically infected, and asymptomatically infected individuals with and without diffusion.

Table 3. Comparison of the present technique with fully explicit Euler scheme in terms of CPU time.

Numerical scheme	Number of iteration	CPU time
Operating splitting technique	25,000	1.268433 Sec
Explicit Euler technique	25,000	1.319197 Sec

4.2.1. Dynamics without diffusion at $x = 0$

In this case, the proposed model (2.1) is simulated without diffusion by assuming $D_S = D_E = D_{I_S} = D_{I_A} = D_V = D_R = 0$. In addition, the effects of the above control interventions are analyzed considering different situations. The dynamics of exposed, symptomatically and asymptomatically infected individuals, in this case are graphically illustrated for the time period 0 to 700 days. A detailed interpretation is presented in Figures 2–4. Figure 2 describes the influence of control measure β on the dynamics of COVID-19. The impact is observed for the estimated baseline value of the effective-contact rate β, without diffusion. Simulations are performed by reducing the baseline value of β to 10, 20 and 30%. It is found that with a 20% decrease in social contacts (β), 53% reduction is observed in infected individuals, while 30% reduction in social contacts, i.e., strengthening lock-down yield to 75% decrease in the number of exposed, symptomatically and asymptomatically infected individuals. Therefore, this analysis shows that enforcing a quarantine policy is beneficial and helps control the spread of infection. The effect of the parameter β_1 on the dynamics of exposed asymptomatic and symptomatic infected individuals is shown in Figure 3. The corresponding dynamics are observed without diffusion for 10, 20 and 30% reduction in β_1 to its estimated baseline value given in Table 2. Simulations show that the number of cases in each category decreased by 23, 45 and 64% respectively. The model (2.1) is simulated without diffusion to investigate the impact of various vaccination rates on the dynamics of exposed, symptomatically and asymptomatically infected individuals. Parameter ψ_v is reduced by 10, 20 and 30% to its estimated baseline value. The resulting plots are shown in Figure 4.

Table 4. Projected peaks of infected individuals generated by model (2.1) without diffusion at $x = 0$.

Parameters	E	I_S	I_A	% Change from Baseline
β (baseline value)	2.1924×10^6	2.5505×10^5	8.7175×10^6	-
10% reduction in β	1.4496×10^6	1.6876×10^5	5.8465×10^6	33.8%
20% reduction in β	7.5062×10^5	8.7437×10^4	3.0607×10^6	65.7%
30% reduction in β	1.7857×10^5	2.0808×10^4	7.3326×10^5	91.8%
β_1 (baseline value)	2.1924×10^6	2.5505×10^5	8.7175×10^6	-
10% reduction in β_1	1.4804×10^6	1.7235×10^5	5.9673×10^6	32.4%
20% reduction in β_1	8.0367×10^5	9.3613×10^4	3.2744×10^6	63.3%
30% reduction in β_1	2.3140×10^5	2.6962×10^4	9.4959×10^5	89.4%
ψ_v (baseline value)	2.1924×10^6	2.5505×10^5	8.7175×10^6	-
10% reduction in ψ_v	1.6864×10^6	1.9629×10^5	6.7663×10^6	23.0%
20% reduction in ψ_v	1.1858×10^6	1.3808×10^5	4.7985×10^6	45.9%
30% reduction in ψ_v	7.0805×10^5	8.2478×10^4	2.8870×10^6	67.7%

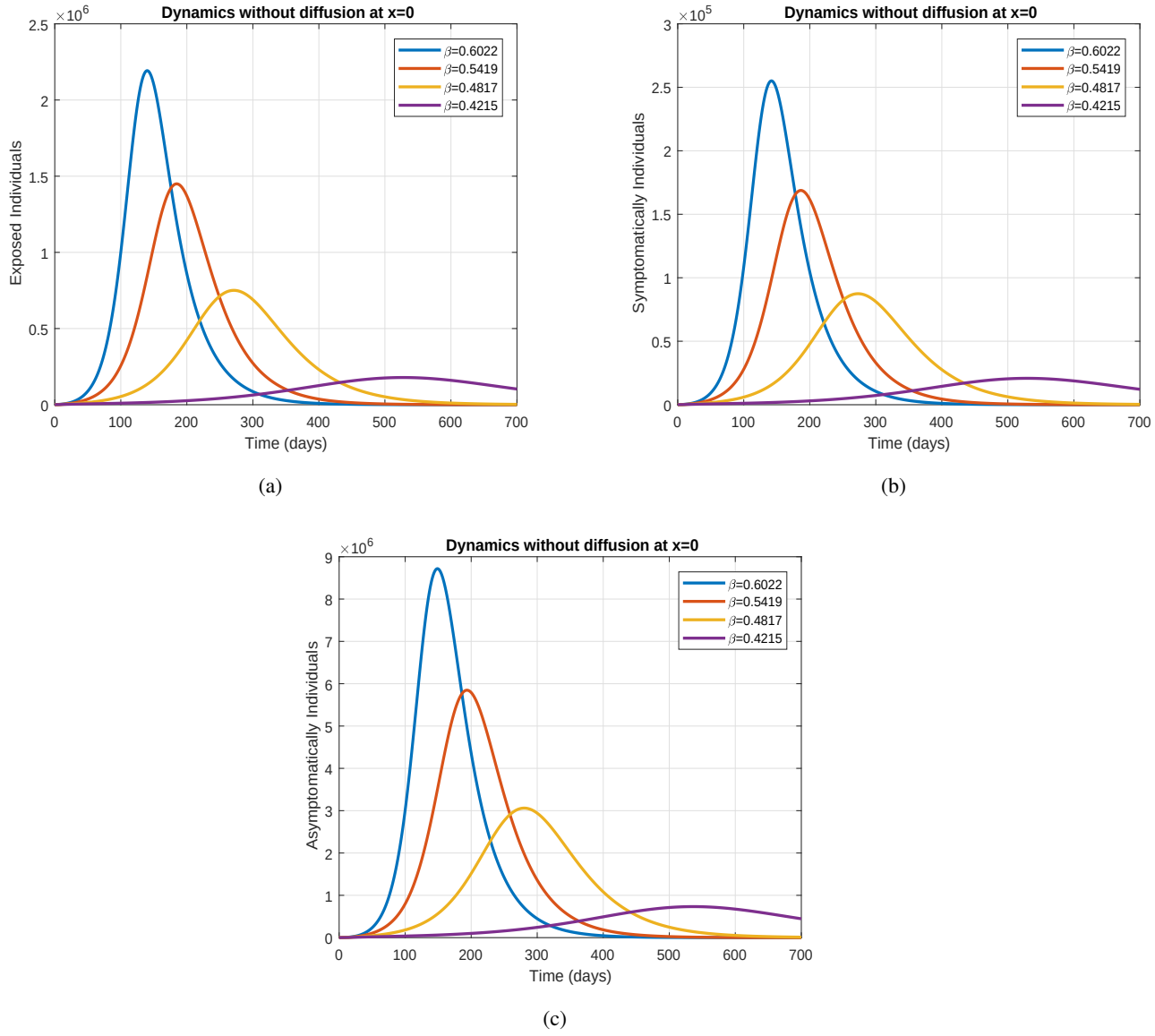

Figure 2. Impact of β on exposed, symptomatically and asymptomatically infected individuals without diffusion.

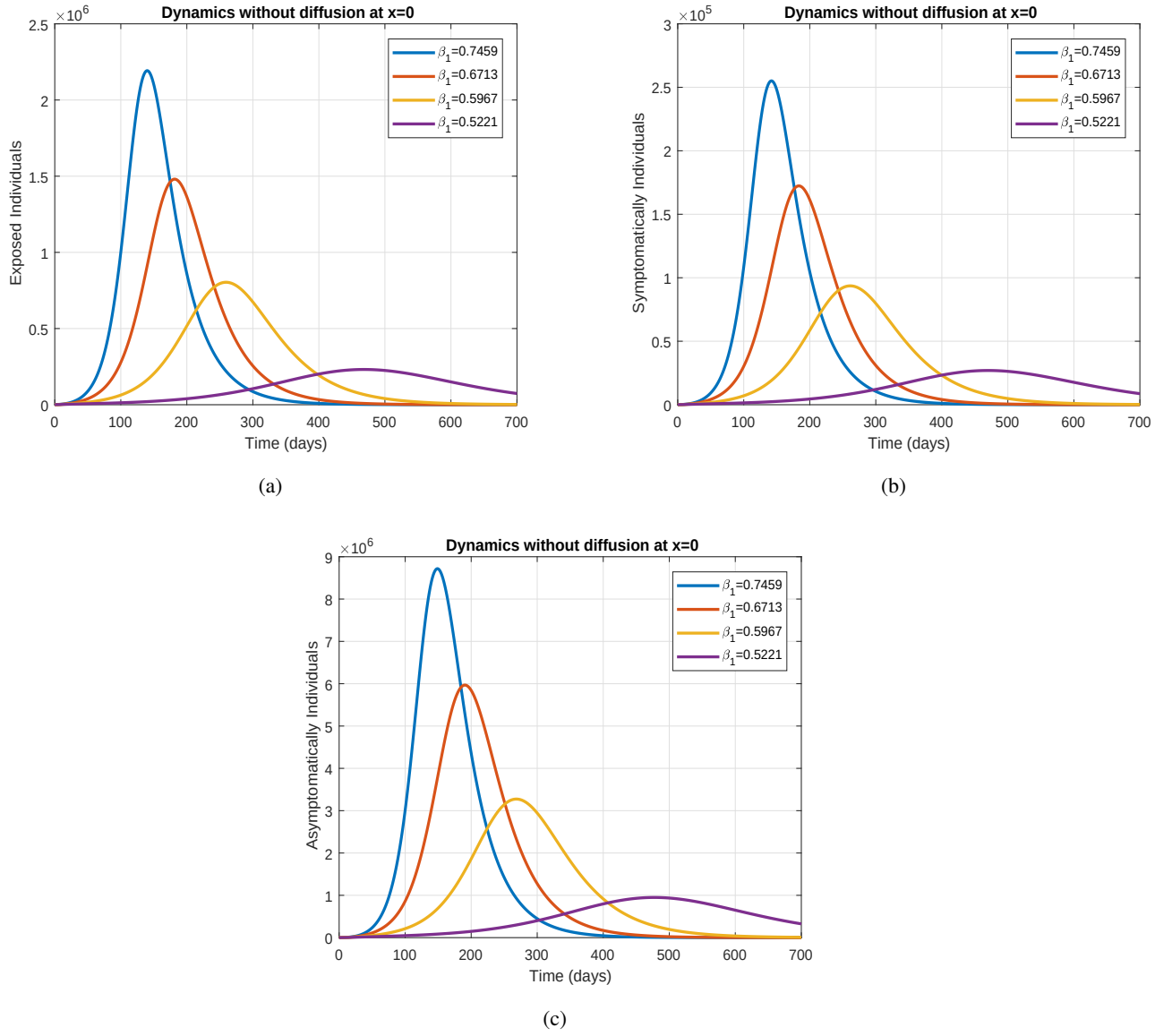

Figure 3. Impact of β_1 on exposed, symptomatically and asymptomatically infected individuals without diffusion.

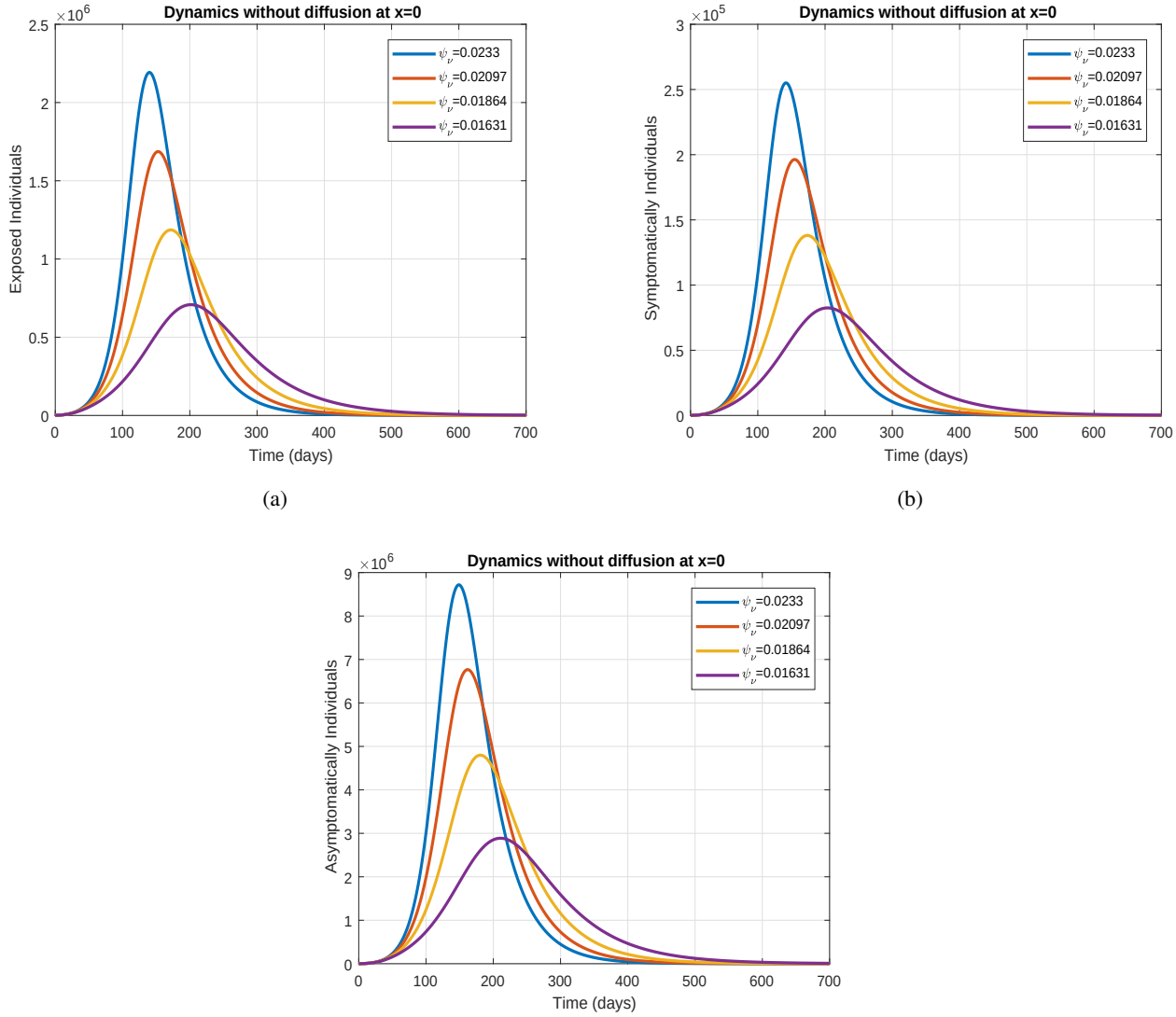

Figure 4. Impact of ψ_ν on exposed, symptomatically and asymptomatically infected individuals without diffusion.

4.2.2. Dynamics with diffusion at $x = 0$

This section presents a simulation of the model (2.1) with diffusion. The values of corresponding diffusion coefficients are assumed as $D_S = 0.00005, D_E = 0.0005, D_{I_S} = 0.0001, D_{I_A} = 0.001, D_V = 0.0001, D_R = 0$. Figure 5 demonstrates the dynamics of the infected population with variation in β in the presence of diffusion. The parameter β is reduced with the same rate discussed in the previous section. By implementing an isolation policy with diffusion, one can analyze that 20% reduction in social contacts yields to 75% decrease in infected individuals. Moreover, with 30% reduction in parameter β the infected individuals are decreased to 93%. Thus, the isolation policy with diffusion is more effective and plays a significant role in controlling the prevalence of infection.

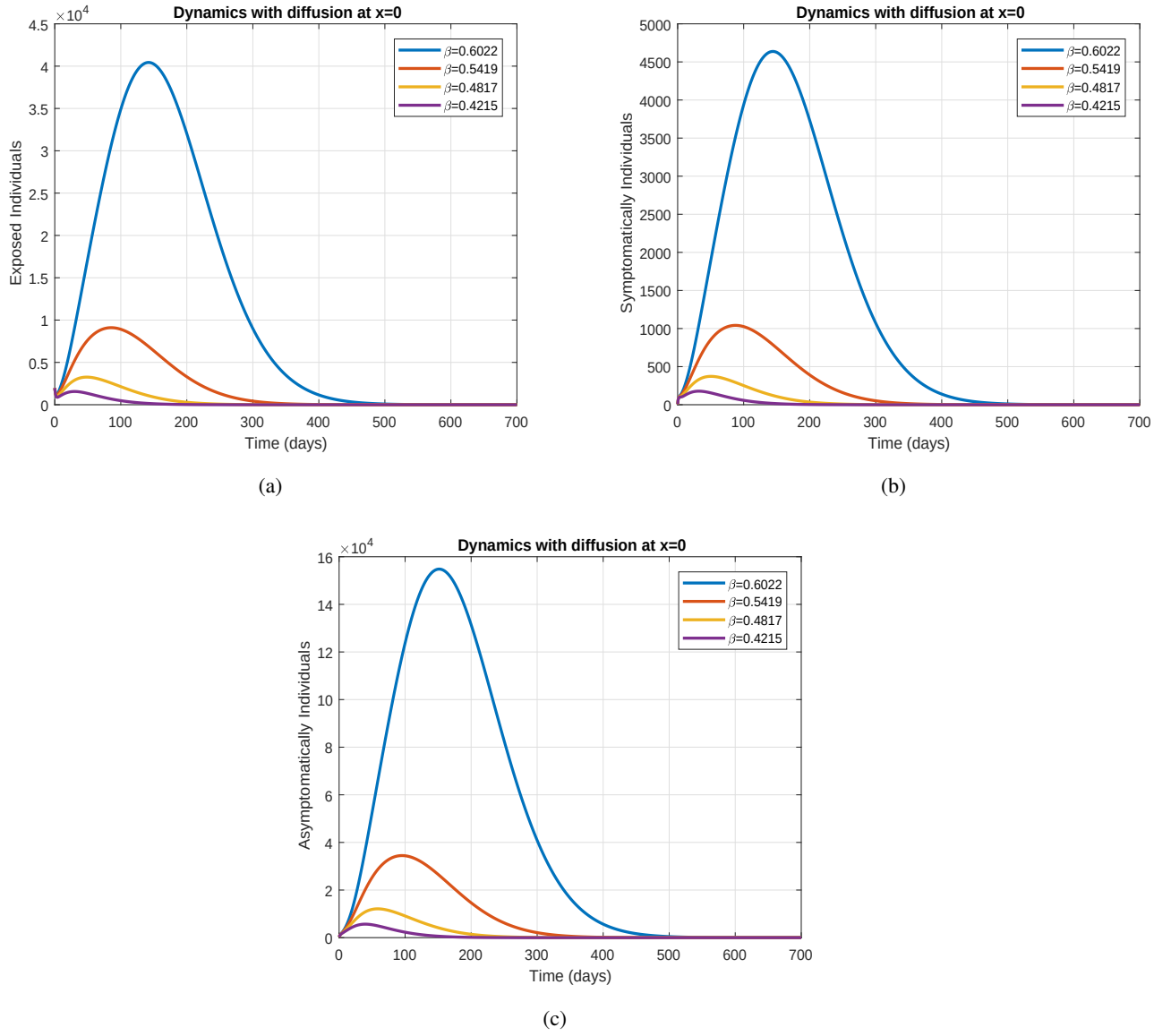

Figure 5. Impact of β on exposed, symptomatically infected individuals with diffusion.

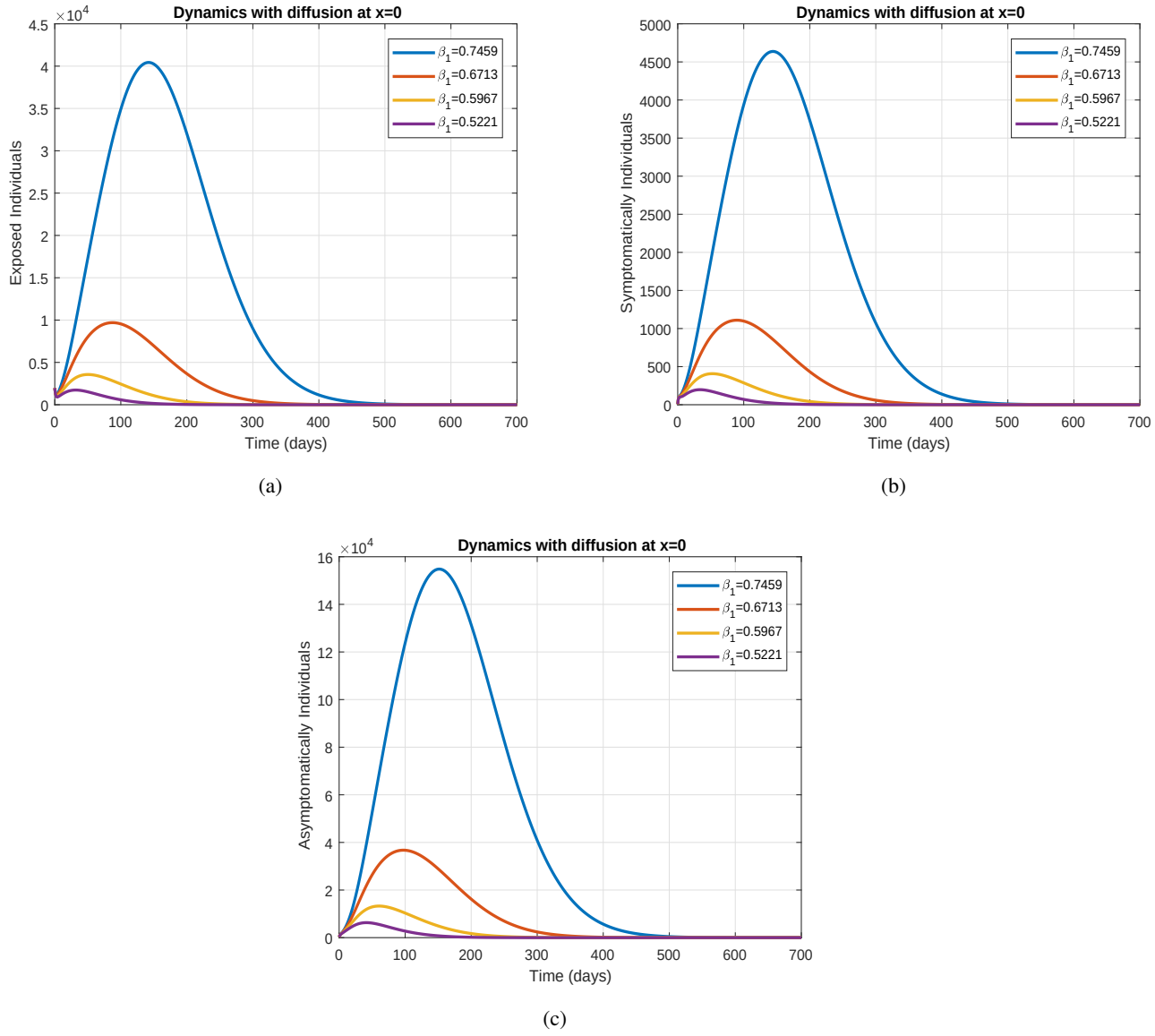

Figure 6. Impact of β_1 on exposed, symptomatically and asymptomatically infected individuals with diffusion.

Figure 6, describes the effect of control intervention β_1 on the disease incidence with diffusion. The simulation results are performed by reducing β_1 to 10, 20 and 30%. One can observe that in this case with a 30% reduction in β_1 the peaks of infected population curvesis reduced to 95.1%. It shows that using the suggested control measure β_1 with diffusion is more beneficial in controlling infection prevalence as compared to without diffusion.

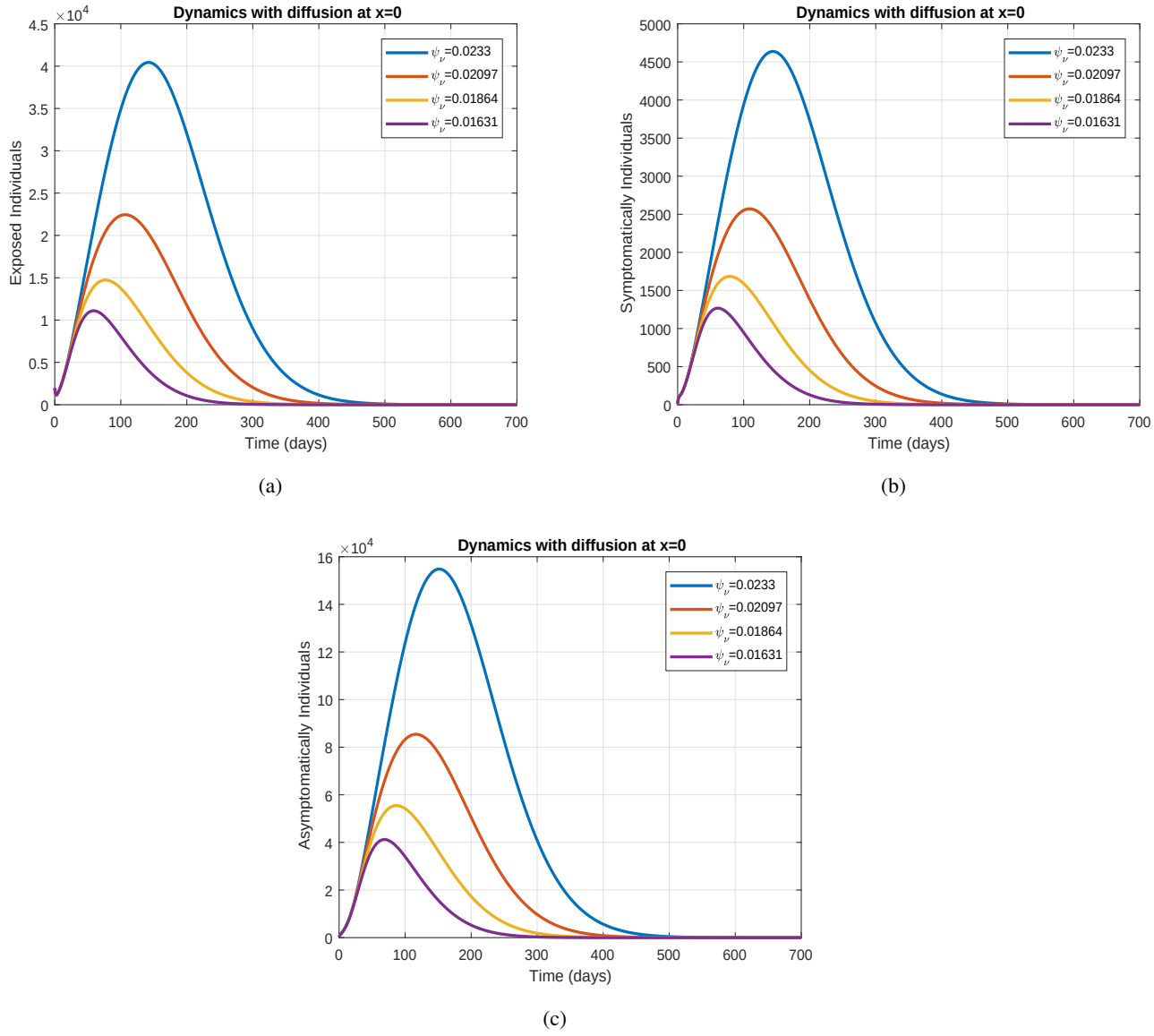

Figure 7. Impact of control intervention ψ_ν on exposed, symptomatically and asymptomatically infected individuals with diffusion.

Table 5. Projected peaks of infected individuals generated by model (2.1) with diffusion at $x = 0$.

Parameters	E	I_S	I_A	% Change from Baseline
β (baseline value)	4.0435×10^4	4.6373×10^3	1.5481×10^5	-
10% reduction in β	9.1015×10^3	1.0415×10^3	3.4668×10^4	77.4%
20% reduction in β	3.2609×10^3	3.722×10^2	1.2107×10^4	91.9%
30% reduction in β	1.9697×10^3	1.778×10^2	5.6651×10^3	95%
β_1 (baseline value)	4.0435×10^4	4.6373×10^3	1.5481×10^5	-
10% reduction in β_1	9.6960×10^3	1.1096×10^3	3.6738×10^4	76%
20% reduction in β_1	3.5689×10^3	4.074×10^2	1.3270×10^4	91%
30% reduction in β_1	1.9697×10^3	1.975×10^2	6.3011×10^3	95.1%
ψ_V (baseline value)	4.0435×10^4	4.6373×10^3	1.5481×10^5	-
10% reduction in ψ_V	2.2449×10^4	2.5712×10^3	8.5421×10^4	44.5%
20% reduction in ψ_V	1.4729×10^4	1.6843×10^3	5.5473×10^4	63.6%
30% reduction in ψ_V	1.1100×10^4	1.2674×10^3	4.1216×10^4	72.5%

Figure 7 describes the impact of variation in parameter ψ_ν on the dynamics of infected individuals. The dynamics are observed in the presence of diffusion. We reduce the estimated value of ψ_V to 10, 20, and 30% and analyze the behavior of exposed, symptomatically, and asymptomatically infected individuals. Simulation results show that reduction in ψ_ν to 30% decreased the population in the respective infected classes to 72.1%. These details are provided in Table 4 and 6.

4.2.3. Dynamics with diffusion at $x = 1$

This section presents a simulation of the model (2.1) with diffusion at $x = 1$. The corresponding plots are shown in Figures 8–10. The time evolutionary trajectories of exposed, symptomatically and asymptomatically infected individuals at $x = 1$ with a reduction in β at different rates are shown in Figure 8. Initially, an increase is observed in the respective curves for the baseline value of β. It is due to the population is diffuses from a higher concentration place to a low concentration region. It has been observed that with diffusion in case of strict lock-down (with a 30% reduction in β) lowest projected peaks are noticed. Figure 9 depicts the influence of β_1 on the dynamics of exposed, symptomatically and asymptomatically infected individuals with diffusion at $x = 1$. The simulation is obtained for a reduction in β_1 with various rates. According to initial condition (2.2) the population is concentrated at the origin and decreases exponentially at $x = 1$. As the population diffuses the concentration increase for $\beta_1 = 0.7459$ at $x = 1$ and significantly reduces with a 30% reduction in β_1. Finally, the impact of ψ_ν(vaccine waning rate) on the dynamics of exposed, symptomatically and asymptomatically infected individuals with diffusion at $x = 1$ is described in Figure 10. By reducing the vaccine waning rate to 10, 20 and 30%, a reasonable decrease is analyzed in the respective compartments of infected individuals.

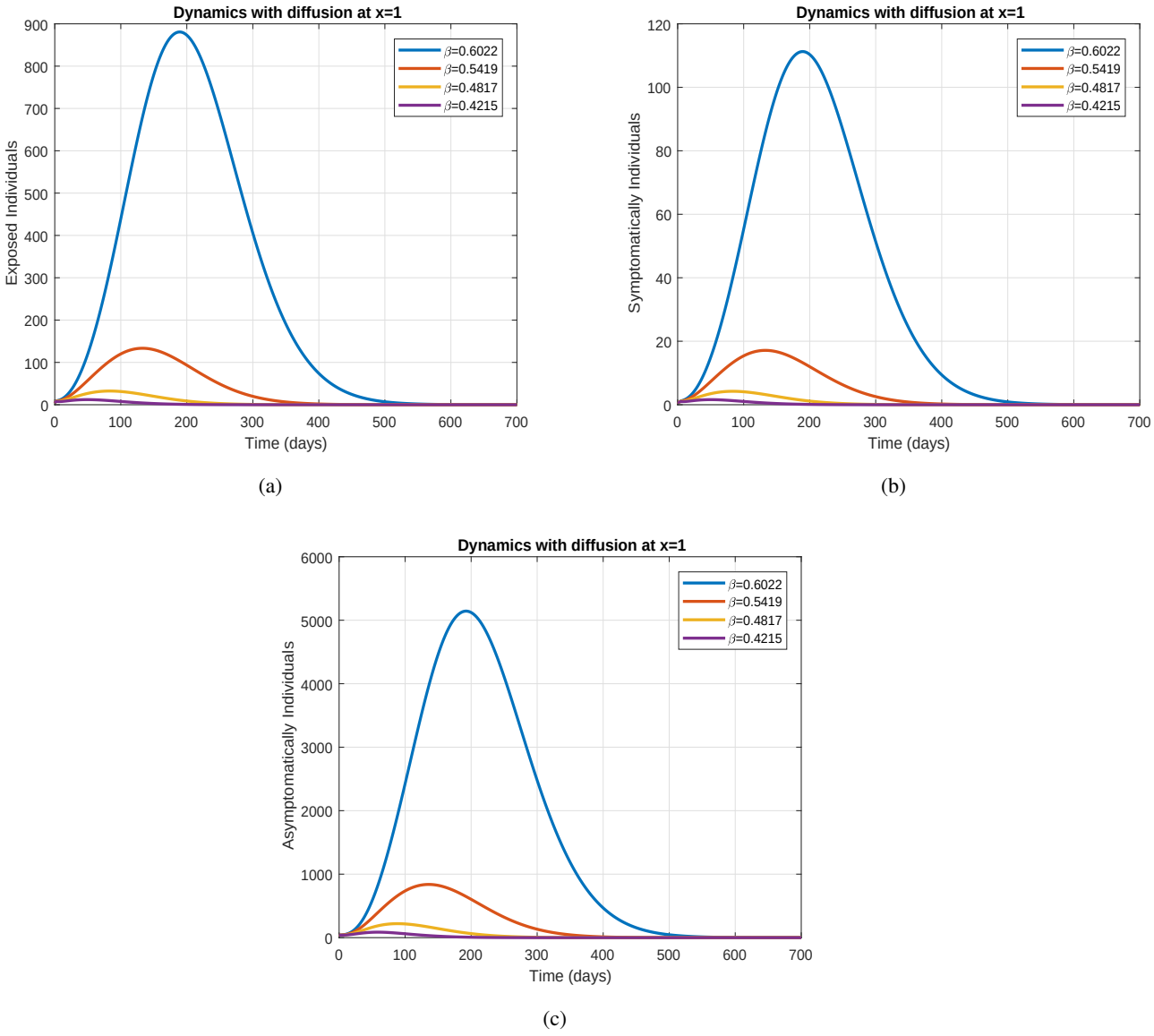

Figure 8. Impact of control intervention β on exposed, symptomatically and asymptomatically infected individuals with diffusion.

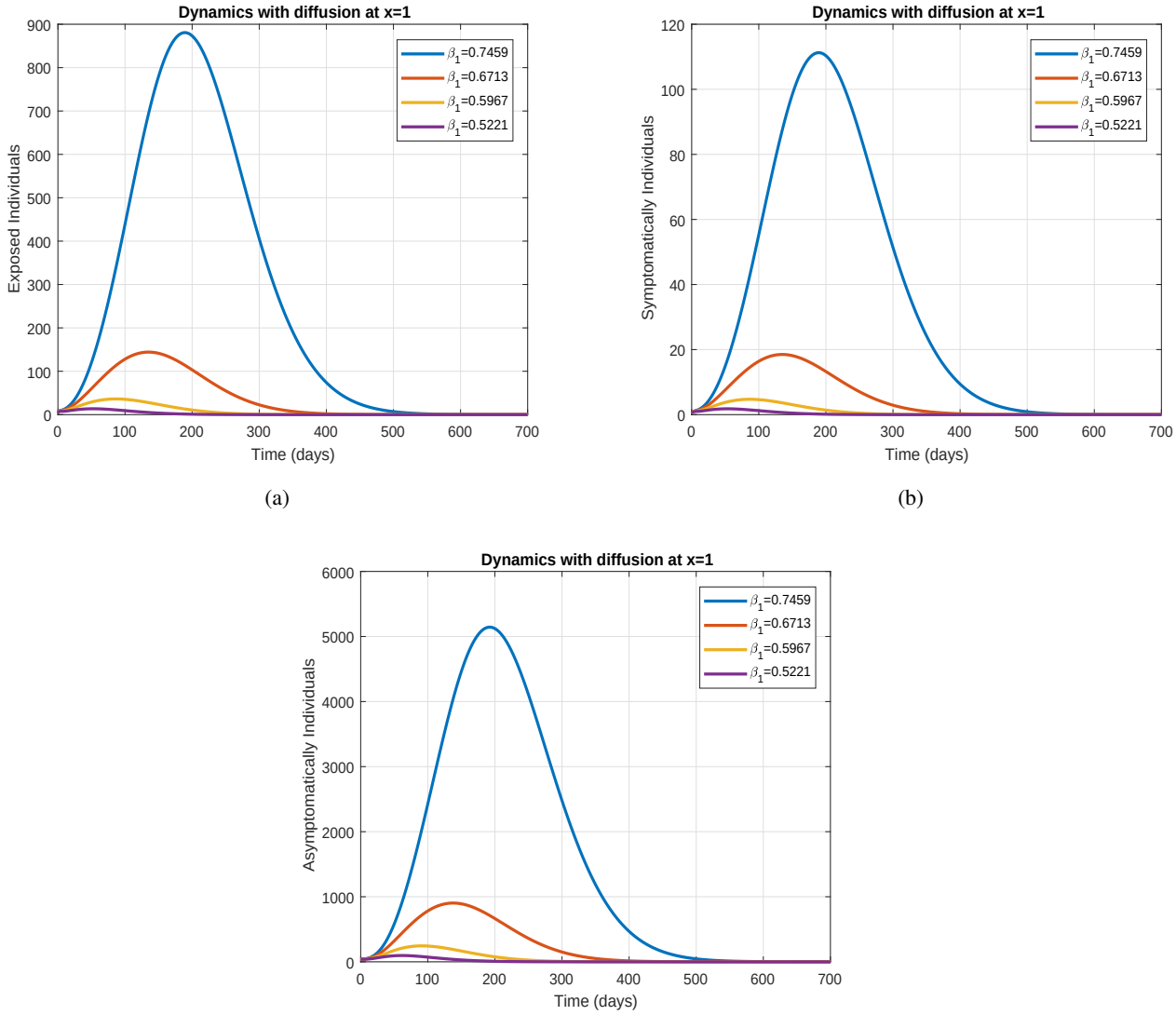

Figure 9. Impact of control intervention β_1 on exposed, symptomatically and asymptomatically infected individuals with diffusion.

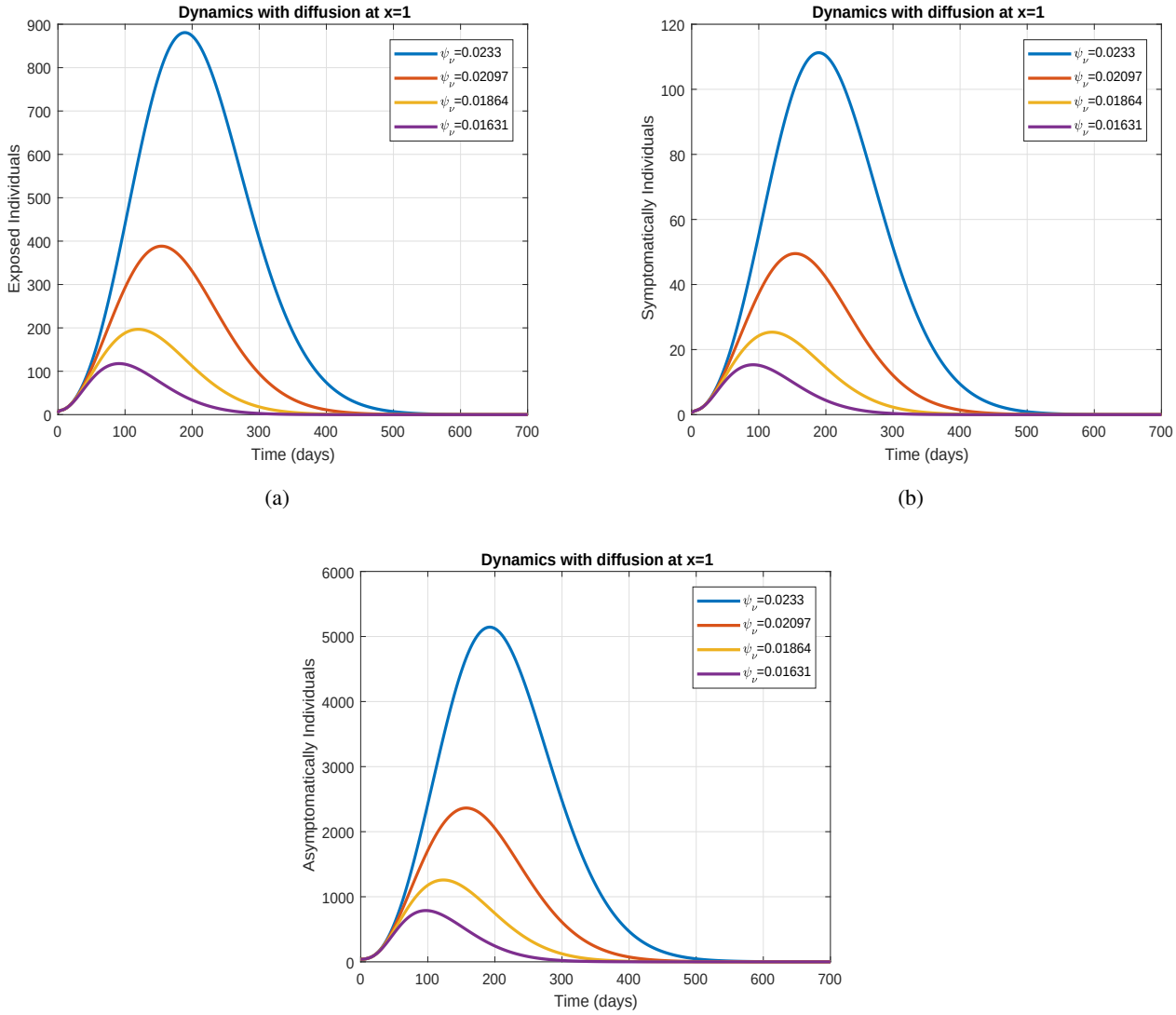

Figure 10. Impact of control intervention ψ_ν on exposed, symptomatically and asymptomatically infected individuals with diffusion.

Table 6. Projected peaks of infected individuals generated by model (2.1) with diffusion at $x = 1$.

Parameters	E	I_S	I_A	% Change from Baseline
β (baseline value)	8.807×10^2	1.112×10^2	5.1435×10^3	-
10% reduction in β	1.334×10^2	17.12	8.380×10^2	84.6%
20% reduction in β	32.35	4.22	2.201×10^2	96.3%
30% reduction in β	12.06	1.60	86.30	98.6%
β_1 (baseline value)	8.807×10^2	1.112×10^2	5.1435×10^3	-
10% reduction in β_1	1.441×10^2	18.49	9.031×10^2	55.9%
20% reduction in β_1	36.14	4.720	2.448×10^2	77.6%
30% reduction in β_1	13.54	1.796	96.72	86.6%
ψ_V (baseline value)	8.807×10^2	1.112×10^2	5.1435×10^3	-
10% reduction in ψ_V	3.883×10^2	49.50	2.3638×10^3	55.4%
20% reduction in ψ_V	1.967×10^2	25.35	1.2577×10^3	77.2%
30% reduction in ψ_V	1.176×10^2	15.33	7.877×10^2	86.2%

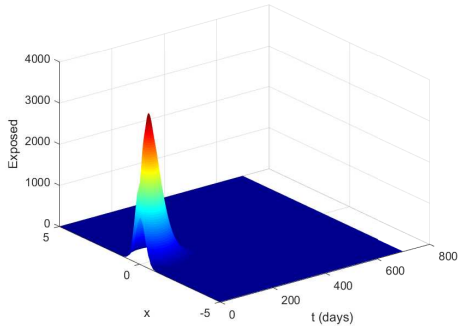

(a)

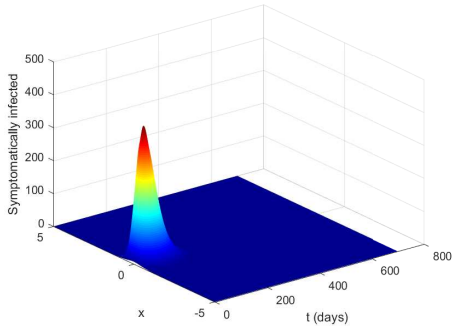

(b)

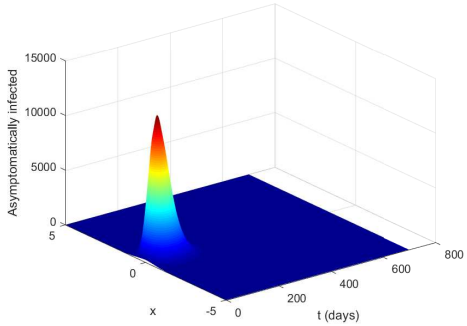

(c)

Figure 11. Mesh plots of exposed, symptomatically and asymptomatically infected individuals with diffusion.

Figure 11 describes mesh plots of model (2.1), which represent the Spatio-temporal evolution of exposed, symptomatically and asymptomatically infected individuals for all time and spatial points in $[5, -5]$. As long as the stability condition given by (4.7) fulfills the proposed scheme produces a stable solution. Moreover the coefficients of diffusivity D_ξ, where ξ represents each of the state variables S, E, I_S, I_A, V and R are chosen so that (4.7) is satisfied. The corresponding mesh plots show the consistent behavior of the proposed operator-splitting finite-difference numerical scheme. Clearly, it preserves the positivity property of the solution, i.e., the solution stays positive for all $t > 0$ and spatial points within the domain of definition $[5, -5]$.

5. Conclusions

In this study, a new mathematical model based on PDEs is constructed to explore the dynamics of COVID-19 outbreak in a spatially heterogeneous environment. The primary focus is to analyze the impact of various significant measures with and without diffusion on the dynamics and control of the pandemic. The basic mathematical properties including existence, uniqueness, positivity, and boundedness of the diffusive vaccinated model are presented. Moreover, the spatio-temporal COVID-19 mathematical model is numerically solved using the finite difference operator-splitting scheme with uniform and non-uniform initial conditions. Based on the derived iterative scheme the model is simulated for various key parameters such as β, β_1, ψ_V with and without diffusion. Further, the dynamics are observed spatially at $x = 0.0$ and $x = 1.0$. The respective results are also shown in tabular form. These results revealed that with diffusion (and at $x = 1$) the reduction in disease transmission coefficients β and β_1 with a 30% rate, the projected peaks of infected individuals reduce upto 98 and 78% respectively as shown in Table 5. The corresponding evolutionary trajectories showed a clear picture of diffusion phenomena and the number of infective individuals significantly reduced with diffusion as compared to without diffusion.

Acknowledgments

This Project was funded by the Denship of Scientific Research (DSR)at King Abdulaziz University, Jeddah, Saudi Arabia under grant no. (G: 394-130-1443). The authors, therefore, acknowledge with thanks DSR for technical and financial support.

Conflict of interest

The authors declare there is no conflict of interest.

Data availability statement

The authors declare that the all data supporting the findings of this study are available within the article.

References

1. Coronavirus disease (COVID-19) pandemic. Available from: https://www.who.int/europe/emergencies/situations/covid-19.
2. Centers for Disease Control and Prevention. Available from: https://www.cdc.gov/coronavirus/2019-ncov/index.html.
3. J. K. K. Asamoah, M. A. Owusu, Z. Jin, F. Oduro, A. Abidemi, E. O. Gyasi, Global stability and cost-effectiveness analysis of COVID-19 considering the impact of the environment: using data from Ghana, *Chaos, Solitons Fractals*, **140** (2020), 110103. 10.1016/j.chaos.2020.110103
4. M. Khan, S. W. Shah, S. Ullah, J. Gómez-Aguilar, A dynamical model of asymptomatic carrier zika virus with optimal control strategies, *Nonlinear Anal.: Real World Appl.*, **50** (2019), 144–170. https://doi.org/10.1016/j.nonrwa.2019.04.006
5. A. Din, Y. Li, F. M. Khan, Z. U. Khan, P. Liu, On analysis of fractional order mathematical model of hepatitis b using atangana–baleanu caputo (abc) derivative, *Fractals*, **30** (2021), 2240017. https://doi.org/10.1142/S0218348X22400175
6. A. Atangana, S. İ. Araz, Nonlinear equations with global differential and integral operators: existence, uniqueness with application to epidemiology, *Results Phys.*, **20** (2021), 103593. https://doi.org/10.1016/j.rinp.2020.103593
7. A. A. Khan, S. Ullah, R. Amin, Optimal control analysis of COVID-19 vaccine epidemic model: a case study, *Eur. Phys. J. Plus*, **137** (2022), 1–25. https://doi.org/10.1140/epjp/s13360-022-02365-8
8. M. Imran, M. Ben-Romdhane, A. R. Ansari, H. Temimi, Numerical study of an influenza epidemic dynamical model with diffusion, *Discrete Contin. Dyn. Syst. -S*, **13** (2020), 2761–2878. https://doi.org/10.3934/dcdss.2020168
9. M. Samsuzzoha, M. Singh, D. Lucy, Numerical study of a diffusive epidemic model of influenza with variable transmission coefficient, *Appl. Math. Modell.*, **35** (2011), 5507–5523. https://doi.org/10.1016/j.apm.2011.04.029
10. M. Jawaz, M. A. ur Rehman, N. Ahmed, D. Baleanu, M. Rafiq, Numerical and bifurcation analysis of spatio-temporal delay epidemic model, *Results Phys.*, **22** (2021), 103851. https://doi.org/10.1016/j.rinp.2021.103851
11. N. Ahmed, M. Ali, M. Rafiq, I. Khan, K. S. Nisar, M. Rehman, et al., A numerical efficient splitting method for the solution of two dimensional susceptible infected recovered epidemic model of whooping cough dynamics: applications in bio-medical engineering, *Comput. Methods Programs Biomed.*, **190** (2020), 105350. https://doi.org/10.1016/j.cmpb.2020.105350
12. N. Haider, Numerical solutions of sveirs model by meshless and finite difference methods, *VFAST Trans. Math.*, **2** (2013), 13–18. https://doi.org/10.21015/vtm.v2i2.128
13. M. Asif, Z. A. Khan, N. Haider, Q. Al-Mdallal, Numerical simulation for solution of seir models by meshless and finite difference methods, *Chaos, Solitons Fractals*, **141** (2020), 110340. https://doi.org/10.1016/j.chaos.2020.110340

14. M. Asif, S. U. Jan, N. Haider, Q. Al-Mdallal, T. Abdeljawad, Numerical modeling of npz and sir models with and without diffusion, *Results Phys.*, **19** (2020), 103512. https://doi.org/10.1016/j.rinp.2020.103512

15. N. Ahmed, M. Fatima, D. Baleanu, K. S. Nisar, I. Khan, M. Rafiq, et al., Numerical analysis of the susceptible exposed infected quarantined and vaccinated (seiqv) reaction-diffusion epidemic model, *Front. Phys.*, **7** (2020), 220. https://doi.org/10.3389/fphy.2019.00220

16. V. Sokolovsky, G. Furman, D. Polyanskaya, E. Furman, Spatio-temporal modeling of COVID-19 epidemic, *Health Risk Anal.*, **2021** (2021), 23–37. https://doi.org/10.21668/HEALTH.RISK/2021.1.03.ENG

17. N. Ahmed, A. Elsonbaty, A. Raza, M. Rafiq, W. Adel, Numerical simulation and stability analysis of a novel reaction–diffusion COVID-19 model, *Nonlinear Dyn.*, **106** (2021), 1293–1310. https://doi.org/10.1007/s11071-021-06623-9

18. P. G. Kevrekidis, J. Cuevas-Maraver, Y. Drossinos, Z. Rapti, G. A. Kevrekidis, Reaction-diffusion spatial modeling of COVID-19: Greece and andalusia as case examples, *Phys. Rev. E*, **104** (2021), 024412. https://doi.org/10.1103/PhysRevE.104.024412

19. L. Zhang, S. Ullah, B. Al Alwan, A. Alshehri, W. Sumelka, Mathematical assessment of constant and time-dependent control measures on the dynamics of the novel coronavirus: an application of optimal control theory, *Results Phys.*, **31** (2021), 104971. https://doi.org/10.1016/j.rinp.2021.104971

20. G. Webb, A reaction-diffusion model for a deterministic diffusive epidemic, *J. Math. Anal. Appl.*, **84** (1981), 150–161. https://doi.org/10.1016/0022-247X(81)90156-6

21. D. Henry, *Geometric Theory of Semilinear Parabolic Equations*, Springer, **840** (2006). https://doi.org/10.1007/BFb0089647

22. E. Avila-Vales, G. E. Garcia-Almeida, A. G. Perez, Qualitative analysis of a diffusive sir epidemic model with saturated incidence rate in a heterogeneous environment, *J. Math. Anal. Appl.*, **503** (2021), 125295. https://doi.org/10.1016/j.jmaa.2021.125295

23. S. Chinviriyasit, W. Chinviriyasit, Numerical modelling of an sir epidemic model with diffusion, *Appl. Math. Comput.*, **216** (2010), 395–409. https://doi.org/10.1016/j.amc.2010.01.028

24. T. Kuniya, J. Wang, Lyapunov functions and global stability for a spatially diffusive sir epidemic model, *Appl. Anal.*, **96** (2017), 1935–1960. https://doi.org/10.1080/00036811.2016.1199796

25. J. LaSalle, Stability theory for difference equations, *Tech. Rep.*, Brown UNIV Providence RI DIV of Applied Mathematics, 1975.

26. Y. Nawaz, M. S. Arif, K. Abodayeh, W. Shatanawi, An explicit unconditionally stable scheme: application to diffusive COVID-19 epidemic model, *Adv. Differ. Equations*, **2021** (2021), 1–24. https://doi.org/10.1186/s13662-021-03513-7

AIMS Press